Biomaterials Science

Acellular and Cellular High-Density, Collagen-Fibril Constructs with Suprafibrillar Organization

Journal:	*Biomaterials Science*
Manuscript ID	BM-ART-10-2015-000443.R1
Article Type:	Paper
Date Submitted by the Author:	22-Jan-2016
Complete List of Authors:	Blum, Kevin; Purdue University, Weldon School of Biomedical Engineering Novak, Tyler; Purdue University, Watkins, Lauren; Purdue University, Weldon School of Biomedical Engineering Neu, Corey; Purdue University, Wallace, Joseph; IUPUI, Biomedical Engineering Bart, Zachary; Indiana University-Purdue University at Indianapolis, Department of Biomedical Egnineering Voytik-Harbin, Sherry; Purdue University, Weldon School of Biomedical Engineering

TITLE

Acellular and Cellular High-Density, Collagen-Fibril Constructs with Suprafibrillar Organization

AUTHORS

Kevin M. Blum[a], Tyler Novak[a], Lauren Watkins[a], Corey P. Neu[a], Joseph M. Wallace[b], Zachary R. Bart[b], Sherry L. Voytik-Harbin[a,c]

AFFILIATIONS

[a]Weldon School of Biomedical Engineering, College of Engineering, Purdue University, West Lafayette, IN 47907, USA

[b]Department of Biomedical Engineering, Indiana University-Purdue University at Indianapolis, Indianapolis, IN 46202, USA

[c]Department of Basic Medical Sciences, College of Veterinary Medicine, Purdue University, West Lafayette, IN 47907, USA

ABSTRACT

Collagen is used extensively for tissue engineering due to its prevalence in connective tissues and its role in defining tissue biophysical and biological signalling properties. However, traditional collagen-based materials fashioned from atelocollagen and telocollagen have lacked collagen densities, multi-scale organization, mechanical integrity, and proteolytic resistance found within tissues *in vivo*. Here, highly interconnected low-density matrices of D-banded fibrils were created from collagen oligomers, which exhibit fibrillar as well as suprafibrillar assembly. Confined compression then was applied to controllably reduce the interstitial fluid while maintaining fibril integrity. More specifically, low-density (3.5 mg/mL) oligomer matrices were densified to create collagen-fibril constructs with average concentrations of 12.25 mg/mL and 24.5 mg/mL. Control and densified constructs exhibited nearly linear increases in ultimate stress, Young's modulus, and compressive modulus over the ranges of 65 to 213 kPa, 400 to 1.26 MPa, and 20 to 150 kPa, respectively. Densification also increased construct resistance to collagenase degradability. Finally, this process was amenable to creating high-density cellularized tissues; all constructs maintained high cell viability (at least 97%) immediately following compression as well as after 1 day and 7 days of culture. This method, which integrates the suprafibrillar assembly capacity of oligomers and controlled fluid reduction by confined compression, supports the rational and scalable design of a broad range of collagen-fibril materials and cell-encapsulated tissue constructs for tissue engineering applications.

INTRODUCTION

In vivo, connective tissue cells reside within a tissue-specific extracellular matrix (ECM) which represents a highly organized network of densely packed fibrous proteins, primarily type I collagen fibrils. It is well established that the collagen suprafibrillar organization and architecture contributes to diversity of tissue structural and functional properties[1]. More recently, the microstructure, mechanical properties (e.g., stiffness), and proteolytic degradation properties of this fibril network have been recognized as powerful morphogens along with the more widely studied soluble factor and cell-cell signalling[2]. Collagen fibrils with their inherent signalling domains instruct fundamental cell behaviors (e.g., proliferation, differentiation, migration, and matrix remodeling) associated with tissue development, maintenance, and repair. As such, it is not surprising that a major goal of tissue engineering and regenerative medicine is the functional design of biomaterials and tissues that replicate these essential multi-scale biochemical and mechanobiology features.

As the major structural protein of tissues, type I collagen demonstrates not only hierarchical, multi-scale organization but also the capacity to self-assemble both *in vivo* and *in vitro*. Within *in-vivo* tissues, the organizational levels of collagen spans various size scales including molecular (10^{-9} m), fibrillar (10^{-6} m), suprafibrillar (10^{-3} m), and tissue/organ (10^{-1} m), with tropocollagen (also known as telocollagen) representing the fundamental collagen polymer building block (Figure 1A). Tropocollagen molecules, which comprise a central triple helical region flanked by short non-helical telopeptide domains, participate in a nucleation and growth mechanism to yield microfibrils, which in turn associate laterally and axially to yield fibrils[3]. Although extensive study has provided a detailed mechanistic understanding of individual collagen fibril assembly (termed fibrillogenesis or fibrillar assembly)[4], much less is known regarding processes associated with higher-order suprafibrillar assembly and organization[5]. This knowledge gap has hindered the rational design and development of collagen-fibril materials and tissue constructs with complex hierarchical architectures and cell-instructive properties found in mature tissues.

To date, collagen-based material and tissue design for both research and medical applications has relied on a limited number of collagen formulations known to vary in purity, solubility, and *in-vitro* self-assembly (polymerization) capacity[6]. Conventional soluble monomer formulations, namely telocollagen and atelocollagen, are commonly used to create low-density, collagen-fibril matrices for three-dimensional (3D) cell culture and tissue engineering applications. These matrices are typically prepared at collagen concentrations of 20 mg/mL or less, largely owing to the limited molecular solubility and/or high viscosity of collagen solutions[7, 8]. Because of their inability to induce supramolecular assembly and higher-order interfibril associations, monomers yield matrices that represent entanglements of long individual fibrils (Figure 1B)[9]. Therefore, even at high densities (10-20 mg/mL), these matrices are associated with poor shape definition, low mechanical integrity, poor handling, cell-induced contraction, and rapid proteolytic degradation[10-13].

In order to overcome the limitations of collagen monomer matrices, methods have been described for creating high-density collagen-fibril constructs that better approximate the structural hierarchy and mechanical properties of mature tissues (Table 1). These methods, which include reverse dialysis, ultracentrifugation, and evaporation, involve generating high concentrations of acid-soluble collagen monomers (>20 mg/mL) followed by neutralization to induce fibrillogenesis. The majority of these approaches were

inspired by current theories and evidence that collagen suprafibrillar organization often mimics geometries described in liquid crystalline states[14]. Unfortunately, these approaches yield a variety of architectures, require long production times (weeks to months), and are not amenable to cell encapsulation. Furthermore, while these high-density constructs support cell adhesion and growth along the surface, migration or infiltration into the material is limited[15, 16].

An alternative 2-step method for achieving high-density collagen-fibril constructs that is more amenable to cell encapsulation involves fibrillar assembly of low concentration monomer solutions followed by unconfined plastic compression and/or capillary fluid flow into absorbent layers to reduce the interstitial fluid content[17]. Here, low-loads (50-60 g or 1.1 kPa) are applied to the top of a collagen matrix (~2-5 mg/mL) to achieve significant fluid reduction (~85-99.8% compressive strain) through a supporting nylon mesh[17, 18]. The resulting densified collagen-fibril sheets, which measure 20 to 100 μm in thickness, are fragile, requiring spiraling to facilitate handling and further testing. They display tensile strength and modulus values of 0.6 ± 0.11 MPa and 1.5 ± 0.36 MPa, respectively, and support 85% viability of encapsulated cells[19]. Additional compression of spiraled constructs improves mechanical integrity but reduces cellular viability[18, 19].

The objective of the present study was to further define robust methods (Figure 2A-B) for creating tunable and scalable self-assembled collagen constructs and cellularized tissues that effectively recapitulate multi-scale structural features, including D-banding and suprafibrillar associations, and functional properties of *in-vivo* soft tissues. The first step involves the use of standardized collagen oligomers to prepare low concentration matrices (<10 mg/mL) with specified and highly reproducible microstructure and physical properties (e.g., intermolecular crosslink content, fibril density, interfibril branches, and proteolytic degradability). Oligomers, which represent soluble aggregates of tropocollagen molecules (e.g., trimers) covalently bonded by their natural intermolecular crosslinks[14], exhibit not only fibrillar but also suprafibrillar assembly (Figure 1B). Next, plastic compression in a confined format is applied to controllably increase the fibril volume fraction or density through forced removal of a portion of the interstitial fluid. Interestingly, we show that this approach is not applicable to collagen-fibril matrices prepared from conventional collagen monomer preparations, telocollagen and atelocollagen. This is largely owing to their limited self-assembly capacity and the inability of the resultant fibril microstructures to sustain or support the associated compressive and fluid shear forces. Collectively, results from this work are important because they support the rational and scalable design of a broad range of collagen constructs and cell-encapsulated tissue constructs for tissue engineering and regenerative medicine applications.

MATERIALS AND METHODS

High-Density Collagen-Fibril Construct Preparation

Type I collagen oligomers were acid solubilized from dermis of market weight pigs as described previously[20]. In brief, pulverized dermis was extracted with sodium acetate to remove soluble non-collagenous proteins and polysaccharides prior to sodium citrate extraction of collagen oligomers. Lyophilized oligomer was dissolved in 0.01 N hydrochloric acid (HCl) and rendered aseptic by chloroform exposure at 4°C. Oligomer concentration was determined using a Sirius Red (Direct Red 80) assay[21]. The oligomer formulation was standardized based upon molecular composition as well as polymerization capacity according to ASTM standard F3089-14[22]. Here, polymerization

capacity is defined by matrix shear storage modulus (G') as a function of oligomer concentration of the polymerization reaction. Commercial acid-soluble rat tail collagen (telocollagen) and pepsin-solubilized bovine dermis collagen (atelocollagen) were obtained from Corning (Corning, NY) and Advanced BioMatrix (Carlsbad, CA), respectively. All collagen solutions were diluted with 0.01 N HCl to achieve desired concentrations and neutralized with 10X phosphate buffered saline (PBS) and 0.1N sodium hydroxide (NaOH) to achieve pH 7.4[9]. Neutralized solutions were kept on ice prior to inducing polymerization by warming to 37°C.

All acellular oligomer collagen-fibril constructs were prepared with an initial starting collagen concentration of 3.5 mg/mL in 2x4x2.5 cm^3 (WxLxH) block molds. After polymerization and incubation at 37°C for 1 hour (tensile testing only) or 18 hours (used for all tests), each construct was subjected to confined compression within the block mold to a final thickness of 2 mm (1.6 mL volume) with a porous polyethylene platen (50 μm pore size; Scientific Commodities, Inc., Lake Havasu City, AZ) at a rate of 6 mm/min. Final construct oligomer concentration was controlled by varying the initial polymerized oligomer volume. More specifically, starting volumes of 1.6 mL, 5.6 mL, and 11.2 mL of 3.5 mg/mL oligomer (initial concentration) were differentially compressed to yield 3.5 mg/mL (no compression), 12.25 mg/mL (71% strain), and 24.5 mg/mL (86% strain) constructs, respectively. Strain calculations were based on initial and final heights of the polymerized matrices. More specifically, constructs created with volumes of 1.6 mL, 5.6 mL, and 11.2 mL had initial measured heights of 2.00 mm, 6.89 mm, and 14.29 mm, respectively. Assuming all oligomer polymerized, densified constructs represented oligomer wet weights (w/w) of 0.6%, 2.1% and 4.2%, respectively, as measured from the masses of hydrated and lyophilized constructs (data not shown). Commercial telocollagen and atelocollagen were polymerized to a collagen concentration of 3.5 mg/mL and allowed to polymerize at 37°C for 18 hours before being subjected to confined compression to 24.5 mg/mL as detailed above for 86% strain.

Collagen Fibril Micro- and Ultra-Structure

The fibril microstructure and ultrastructure of the oligomer constructs were visualized using confocal reflection microscopy[23], cryogenic scanning electron microscopy (cryo-SEM)[24], and atomic force microscopy (AFM). Confocal reflection microscopy was performed using an Olympus Fluoview FV-1000 confocal system adapted to an Olympus IX81 invested microscope with a 60X UPlanSApo water immersion objective (Olympus, Tokyo, Japan). Cryo-SEM images of samples were obtained using an FEI NOVA nanoSEM 200 (FEI, Hillsboro, OR) varying between an Everhart-Thronley (<10,000x magnification) or immersion lens (>10,000x magnification) detector. Samples were quick frozen by submersion into critical point liquid nitrogen, transferred to a CT1000 cold-stage attachment (Oxford Instruments North America, Inc., Concord, MA), and sublimated under vacuum for 15 minutes before sputter coating and imaging.

To facilitate AFM analysis of collagen fibril D-periodic banding, collagen formulations were polymerized on glass at 0.5 mg/ml, extensively rinsed with water, and then air dried. Samples were imaged in air using a Bruker BioScope Catalyst AFM (Bruker Corporation, Santa Barbara, CA) as described previously[25]. In brief, images were acquired in a peak force tapping mode using ScanAsyst Fluid+ probes (silicon tip, silicon nitride cantilever, nominal tip radius 2 nm and nominal stiffness of 0.7 N/m). From each sample (*n=4* per group), 15-20 fibrils at each of 2 locations were imaged and analyzed (~150 total fibrils per group). Two-dimensional fast fourier transforms were performed

and the primary peak from the 2D power spectrum was analyzed to determine the value of the D-periodic spacing for individual fibrils.

Mechanical Testing

Tensile testing was performed on dog-bone shaped collagen constructs with a gauge length, width, and thickness of 26 mm, 4 mm, and 2 mm, respectively (*n*=*7*). Samples were maintained in PBS prior to mechanical testing in ambient air. The duration of mechanical testing from set up to completion was less than 10 seconds and sample dehydration was not observed. All samples were tested in uniaxial tension to failure at a near physiological strain rate of 38.4 %/second using a servo electric materials testing system (Testresources, Shakopee, MN)[26]. Stress measurements were obtained using a 44.5 N load cell (LPM 512, Cooper Instruments, Warrenton, VA) at a sampling rate of 100 Hz. Engineering Young's (tensile) modulus (E_T) was calculated from the linear region of the stress strain curve. Ultimate stress ($\boldsymbol{\sigma}_U$) represented peak stress experienced by the sample, and failure strain (ε_f) was the strain at which constructs experienced total failure.

Proteolytic Degradability

Proteolytic degradation was measured by measuring compressive modulus and hydroxyproline content of constructs before and after 2-hour exposure to bacterial collagenase type IV (31.2 U/mL; Worthington, Lakewood, NJ)[27, 28]. Collagen constructs prepared at 3.5, 12.25, and 24.5 mg/mL were punched to form cylinders with diameter and thickness of 1 cm and 2 mm, respectively. Constructs were tested in unconfined compression at 17%/second to 75% strain using a servo electric materials testing system (Testresources, Shakopee, MN) adapted with a 44.5 N load cell (LPM 512, Cooper Instruments, Warrenton, VA). Compressive modulus was calculated as the slope of the linear region of the stress-strain curve (*n*=*7*). Control and collagenase-treated constructs were then subjected to a spectrophotometric-based hydroxyproline assay (Sigma Aldrich) to determine collagen content.

Cellularized High-Density Tissue Construct Preparation

Low-passage human adipose-derived stem cells (hASC) were obtained from Zen-Bio (Research Triangle Park, NC). Cells were cultured in Dulbecco's Modified Eagle Medium (DMEM; Life Technologies, Carlsbad, CA) with 10% fetal bovine serum (FBS), 100 U/mL penicillin, and 100 U/mL streptomyosin (Invitrogen, Grand Island, NY). The hASC were grown and maintained in a humidified environment of 5% carbon dioxide in air at 37°C. Cells were kept below 80% confluence and used in experiments at passage 6 to 9.

To create cellularized, high-density, collagen-fibril constructs, hASC were added to neutralized oligomer solutions (3.5 mg/mL) and polymerized for 15 minutes at 37°C (Figure 7). Tissue constructs representing different volumes, specifically 50 µL, 175 µL, or 350 µL, were created in glass-bottom 96-well plate (Corning, Corning, NY). Constructs were densified to 1.5 mm final thickness (50 µL volume). Final hASC density within constructs was 5×10^5 cells/mL. Immediately following densification, 200 µL of medium was added to each well and tissue constructs were maintained in a humidified environment at 37°C and 5% CO_2 in air with medium changes every 24 hours. Cell viability was measured at 2 hours, 1 day, and 7 days after construct densification and compared to undensified control constructs by staining with calcein-AM (Life Technologies) and propidium iodide (Sigma-Aldrich). Confocal image stacks of 25 images at gaps of 2 µm (50-µm total thickness) were collected and used for live/dead analysis

via Imaris Iso Surface software (Bitplane, St. Paul, MN; *n=3*). Cell morphology and cell-matrix interactions were assessed at day 2 by staining constructs with phalloidin (Molecular Probes, Eugene, OR) and Draq5 (Biostatus Limited, Leicestershire, United Kingdom) for visualization of F-actin and the nucleus, respectively.

Statistical Analysis

Statistical analysis was performed using Minitab statistical software. One-way ANOVA was applied across collagen concentrations (3.5, 12.25, and 24.5 mg/mL) with a Tukey post-hoc test to determine differences in mean values. In cases where population variances were not equal (ultimate stress, Young's modulus, and compressive modulus), a Kruskal-Wallis test was performed in place of ANOVA with post-hoc 2-sample T-tests assuming non-equal population variances. Mean D-periodic spacing values were compared using an ANOVA and a post-hoc Holm-Sidak test. To examine differences in the distribution of fibril D-periodic spacing values, the Cumulative Distribution Function (CDF) of each group was computed and statistically compared using a Kolmogorov-Smirnov (KS) test. A critical global p-value of 0.05 was used.

RESULTS AND DISCUSSION

Type I collagen oligomers demonstrate *in-vitro* fibrillar and suprafibrillar assembly

Recently we described oligomers, a soluble collagen subdomain that falls between molecular and fibrillar size scales[9, 29]. As shown in Figure 1B, oligomers represent tissue-derived aggregates of tropocollagen molecules (e.g., trimers). They maintain their natural intermolecular crosslinks and have higher average molecular weights than monomers, which likely contributes to their uncommon self-assembly properties. Oligomers exhibit rapid fibril and suprafibrillar self-assembly yielding highly interconnected collagen-fibril matrices[10] with dramatically improved shape retaining capacity, mechanical integrity, resistance to cell-induced contraction, and reduced proteolytic degradation compared to their monomer counterparts[14, 30]. In fact, the shear storage modulus range reported for oligomer matrices prepared at 0.5-4 mg/mL was 40-1500Pa, while that for telocollagen and atelocollagen preparations was 2-300Pa and 2-50Pa, respectively[10].

AFM analysis revealed that component fibrils within oligomer and telocollagen but not atelocollagen matrices displayed highly regular and prominent D-periodic spacing patterns (Figure 3A-C). Although the atelocollagen formulation and polymerization conditions used in the present study produced fibrils with some D-banding evidence, spacing patterns lacked necessary regularity and prominence for AFM quantification. Non-helical telopeptide regions have been shown to help guide correct periodic assembly and crosslinking of assembling fibrils[3, 31]. Telopeptide removal, as occurs with pepsin or pronase digestion, results in loss of unidirectional molecular packing and fibril diameter uniformity[32, 33]. Quantitative analysis revealed that mean fibril D-periodic spacing for telocollagen and oligomer matrices were statistically similar ($p=0.299$), with values of 66.1 ± 0.1 nm (n=4; 164 fibrils) and 66.7 ± 0.9 nm (n=4; 144 fibrils), respectively. However, evaluation of D-spacing distributions, when plotted in histogram (Figure 3D) or cumulative distribution (Figure 3E) formats, showed a statistically significant ($p<0.001$) rightward shift toward higher values for oligomer compared to telocollagen. Numerous reports indicate that D-spacing values are consistently shifted toward higher values in situations where crosslinking (whether enzymatic, non-enzymatic, or chemically-induced) is higher[34-37]. Collectively, these findings further

support the notion that oligomers with their inherent intermolecular crosslinks assist in precise molecular ordering and alignment during self-assembly[5].

Oligomer but not telocollagen and atelocollagen matrices support densification via confined compression

To prepare collagen-fibril constructs with densities approaching *in-vivo* soft tissues, low-density oligomer matrices were subjected to controlled fluid reduction via forced flow using confined compression. Starting concentration of the constructs was held constant but the strain levels varied from (0 to 71% to 86%) to prepare constructs representing final densities of 3.5 mg/mL, 12.25 mg/mL, and 24.5 mg/mL. Interestingly, confined compression of oligomer matrices yielded an intact tissue-like material, 2 mm in thickness, with higher-order interfibril associations (Figure 4B). Telocollagen and atelocollagen preparations, on the other hand, could not sustain the compression-induced fluid shear forces and yielded inhomogenous slurries of fluid and fibrillar fragments (Figure 4B). Both confocal reflection and cryo-SEM imaging confirmed that the fibril-microstructure and ultrastructure of the densified oligomer constructs remained intact and highly porous (Figure 5). The progressive increase in fibril density (fibril volume fraction) observed with densification was most evident from confocal reflection microscopy images (Figure 5A-C), while cryo-SEM highlighted the maintenance of a highly porous fibril microstructure (Figure 5D-E). More detailed qualitative and quantitative studies of densified oligomer[38] and telocollagen constructs[17] indicate that bundling or aggregation of smaller diameter fibrils contribute significantly to the observed changes in their hierarchical structure and mechanical properties. Collectively, these results demonstrate the critical contribution of suprafibrillar assembly to the overall hierarchical organization and material properties of collagen-fibril constructs.

Confined compression of oligomer matrices improves mechanical properties in a density dependent fashion

The most notable shortcomings of commercial collagen-based materials, whether fashioned from soluble or insoluble collagens, include poor mechanical integrity and rapid proteolytic degradation[39]. Various approaches, including cell-induced compaction[40] and chemical and physical crosslinking[41] have been routinely applied to improve these properties. Unfortunately, cell-based methods produce only modest improvements in these performance parameters[40] and exogenous crosslinking is often associated with deleterious effects on biocompatibility and inherent biological signalling capacity[42]. The present work demonstrates how controlled fluid reduction of oligomer matrices using confined compression significantly improves mechanical properties and proteolytic resistance in absence of exogenous crosslinking and other processing. It is important to note that all collagen-fibril constructs were stored in PBS prior to mechanical testing It is important to note that all collagen-fibril constructs were stored in PBS prior to mechanical testing and demonstrated no discernible swelling over the range of densities studied. Such results are consistent with previous reports involving unconfined plastic compression of telocollagen matrices[17] indicating that microstructure-mechanical properties are sufficient to prevent deformation induced by osmotic forces (driven by collagen fixed charge density)[43].

Since the extent of polymerization and stress-strain behavior of reconstituted collagen matrices has been shown to be dependent upon polymerization time[9], oligomer matrices were polymerized for 1 hour or 18 hours, prior to densification and follow-up tensile testing. Despite the polymerization time, confined compression resulted in high-density,

collagen-fibril constructs with increased ultimate stress and Young's modulus (Figure 6). Polymerization time did not significantly affect ($p>0.05$) mean mechanical property values; however, 12.25 mg/mL and 24.5 mg/mL constructs polymerized for 18 hours showed improved reproducibility as evidenced by reduced standard deviations. As such, an 18-hour polymerization time was applied for all follow-up experiments. Since high-density constructs involved polymerization of larger initial collagen volumes at 37°C, it is plausible that heat transfer properties were altered, affecting polymerization rate and outcomes. Additional studies are needed to further define the relationship between the extent of polymerization as a function of collagen volume and polymerization time.

Measured mechanical properties for oligomer constructs prepared at 3.5, 12.25, and 24.5 mg/mL are summarized in Figure 6 and Table 2. Both ultimate stress and Young's modulus increased in as statistically significant fashion with oligomer content ($p<0.05$). All samples, regardless of densification, failed near 28% strain (Table 2). These measured values fall above the range reported for human adipose tissue (0.5-25 kPa), and within reported ranges for several human soft tissues including artery and vein (0.6-3.5 MPa), cornea (0.1-11.1 MPa), and dermis (0.6-15 MPa)[44, 45]. The significant contribution of higher-order suprafibrillar assembly to the mechanical properties of densified oligomer constructs also is evident upon comparison of results obtained in the present study with those obtained previously with conventional monomer formulations. Telocollagen densified via passive absorption of fluid required 98% fluid removal and densities of nearly 100 mg/mL to yield strength and Young's modulus values observed with 24.5 mg/mL oligomer constructs, and the resulting materials had a thickness of less than 100 um[17]. Furthermore, conventional collagen materials treated with exogenous chemical crosslinking typically exhibit, on the high end, Young's modulus values of roughly 15-200 kPa, orders of magnitude weaker than the 400 kPa-1.2 MPa observed with oligomer constructs prepared in absence of exogenous crosslinking[46].

Densification of oligomer matrices improves *in-vitro* proteolytic resistance

Densification of oligomer constructs was also found to modulate *in-vitro* proteolytic degradation properties as measured using collagenase from *Clostridium histolyticum*. While the specificity of mammalian collagenase is more limited compared to bacterial collagenase, good empirical correlation between the extent of *in-vitro* degradation by bacterial collagenase and *in-vivo* degradation by mammalian collagenase has been documented[27]. Qualitative and quantitative assessment of collagenase degradation (Figure 7) indicated that the extent of densification affected the degradation rate.

Following 2-hour exposure, the 3.5 mg/mL construct was nearly entirely degraded, while the 12.25 mg/mL and 24.5 mg/mL constructs showed markedly higher collagenase resistance (Figure 7A). Interestingly, 3.5 mg/mL and 12.25 mg/mL constructs appeared to develop small degraded regions throughout the surface area of the construct. In contrast, degradation of the 24.5 mg/mL construct appeared more concentrated to the periphery. Proteolytic degradation of the constructs also was defined and compared quantitatively based on the change in compressive modulus before and after 2-hr collagenase treatment (Figure 7B). Collagenase-treated 3.5 mg/mL constructs showed a dramatic reduction in compressive modulus to 6.7% of untreated controls. In contrast, 12.25 mg/mL and 24.5 mg/mL samples showed significantly reduced levels of collagenase degradation with compressive modulus values of 47% and 71% of untreated controls (Figure 7C). These collagenase-induced changes in mechanical performance correlated well with collagen content as measured using conventional hydroxyproline assay (Figure 7D).

hASC encapsulated in densified oligomer constructs exhibit high viability and construct-dependent morphologies

As stated previously, the majority of exogenous crosslinking methods as well as approaches used to achieve high-density collagen constructs compromise cell viability and/or are not amenable to cell encapsulation. To date, plastic unconfined compression of cellularized, telocollagen matrices has shown the most success at maintaining cell viability in densified constructs[47]. Here, we document the utility of our controlled confined compression process for creating cellularized, high-density tissue constructs. For these studies, low-density oligomer constructs embedded with hASC were first created and then compressed to various strain levels (Figure 2B). Human ASC were chosen since they represent a potential autologous therapeutic cell population[48, 49]. Cell viability was assessed 2 hours, 1 day, and 7 days after densification and compared to undensified control constructs; morphology and F-actin (phalloidin) distribution were assessed after 2 days.

Cell viability for control 3.5 mg/mL constructs and densified 12.5 mg/mL and 24.5 mg/mL constructs were statistically similar ($p>0.05$) measuring 98.4±1.4%, 99.0±1.1%, and 97.2±1.1%, respectively. This suggested that compressive loading and associated fluid shear forces had no immediate detrimental effects on resident cells. Furthermore, this high cell viability within densified constructs was maintained at 1 day and 7 days of culture (Figure 8). In fact, no statistical difference in viability between densified and control constructs was observed at any timepoint ($p>0.05$). Interestingly, as shown in Figure 8, hASC did exhibit time- and construct-dependent changes in their morphology. Spindle-shaped hASC were noted as early as 1 day in 3.5 mg/mL constructs, while the majority of cells in high-density 24.5 mg/mL constructs maintained a more stellate or rounded shape. Although the total cell number appeared to increase in all constructs over the 7-day culture period, additional studies are needed to accurately assess differences in matrix-induced cell proliferation.

Visualizing F-actin organization (phalloidin) within hASCs encapsulated within the various high-density collagen-fibril constructs provided additional insights regarding these cell-matrix interactions and associated mechanobiology signalling. The actin cytoskeleton is well recognized for its role in cell morphology as well as establishing physical linkage between the cell interior and collagen fibrils of the ECM through focal adhesions[50]. In the control 3.5 mg/mL constructs, hASC were spindle-shaped and elongated with prominent actin stress fibers along their long axis, while cells encapsulated within 12.25 mg/mL and 24.5 mg/mL constructs responded to the progressive increase in fibril density and associated matrix stiffness by taking on more stellate and polygonal morphologies, respectively (Figure 9). Furthermore, actin stress fibers became less prominent with the adoption of a more uniformly-distributed, punctate F-actin staining pattern. Collectively, these morphology and cytoskeletal changes are consistent with previous reports, and reflect modulation of the cell-matrix tensional balance as occurs with matrices and substrates that are able to resist cell contractile forces[51, 52]. Additional long-term studies are needed to define how these apparent differences in cell-matrix mechanobiology signalling contribute to distinct cell fate outcomes, including phenotype and function.

CONCLUSIONS

The development of functional tissue constructs for research and medical applications requires an in-depth understanding of how cells interact and respond to the surrounding

ECM. A key finding of this work is the benefit of oligomers and their associated suprafibrillar assembly capacity for creating acellular or cellular collagen-fibril constructs with tissue-like appearance, handling, and performance. Densification, also referred to as plastic compression, of oligomer matrices via confined compression supported the irreversible removal of specified portions (71-86%) of the interstitial fluid component, reproducibly creating constructs with collagen densities, higher-order interfibril associations, and mechanical properties of soft connective tissues[44]. These constructs are prepared without the use of any exogenous crosslinking chemicals or matrix destroying processes, retaining collagen's multi-scale structural features and inherent biological signalling capacity. The application of confined versus unconfined compression to collagen-fibril constructs with higher intrinsic mechanical stability provides additional control over the direction, extent, and rate of fluid removal, allowing various complex fibril architectures to be created in a highly reproducible fashion. More specifically, detailed studies show that fibril density gradients within oligomer matrices are highly dependent upon the level of applied strain, strain rate, and direction of forced fluid removal[38]. This new hierarchical design strategy involving self-assembling oligomers and controlled fluid reduction by confined compression effectively expands the range of acellular and cellular tissue constructs that can be rationally designed for medical and research applications including tissue engineered medical products and *in-vitro* 3D tissue systems for basic research, drug discovery, and toxicity testing.

ACKNOWLEDGEMENTS

This work was funded in part by the Purdue University Office of the Vice President for Research Incentive Grant Funds (SLH, CPN), the Purdue University Charles C. Chappelle Fellowship (KB), and the NSF Graduate Research Fellowship Program under Grant No. DGE-0833366 (TN).

NOTES AND REFERENCES

1. D. J. S. Hulmes, *J Struct Bio*, 2002, **137**, 2–10.

2. T. Mammoto, A. Mammoto and D. E. Ingber, *Cell Dev Bio*, 2013, **29**, 27-61.

3. K. Gelse, E. Poschl and T. Aigner, *Adv Drug Deliv Rev*, 2003, **55**, 1531-1546.

4. D. L. Christiansen, E. K. Huang and F. H. Silver, *Matrix Bio*, 2000, **19**, 409–420.

5. A. J. Bailey, R. G. Paul and L. Knott, *Mech Ageing Dev*, 1998, **106**, 1-56.

6. L. C. Abraham, E. Zuena, B. Perez-Ramirez and D. L. Kaplan, *J Biomed Mater Res, Part B*, 2008, **87**, 264-285.

7. P. Fratzl, *Collagen - Structure and Mechanics*, Springer, New York, 1 edn., 2015.

8. G. C. Wood and M. K. Keech, *Biochem J*, 1960, **75**, 588-598.

9. B. A. Roeder, K. Kokini, J. E. Sturgis, J. P. Robinson and S. L. Voytik-Harbin, *J Biomech Eng*, 2002, **124**, 214-222.

10. S. Kreger, B. Bell, J. Bailey, E. Stites, J. Kuske, B. Waisner and S. Voytik-Harbin, *Biopolymers*, 2010, **93**, 690-707.

11. A. O. Brightman, B. P. Rajwa, J. E. Sturgis, M. E. McCallister, J. P. Robinson and S. L. Voytik-Harbin, *Biopolymers*, 2000, **54**, 222-234.

12. S. T. Kreger and S. L. Voytik-Harbin, *Matrix Bio*, 2009, **28**, 336–346.

13. J. L. Puetzer and L. J. Bonassar, *Acta Biomater*, 2013, **9**, 7787–7795.

14. C. F. Whittington, E. Brandner, K. Y. Teo, B. Han, E. Nauman and S. L. Voytik-Harbin, *Microsc Microanal*, 2013, **19**, 1323-1333.

15. K. R. Johnson, J. L. Leight and V. M. Weaver, *Methods Cell Biol*, 2007, **83**, 547-583.

16. A. Nyga, M. Loizidou, M. Emberton and U. Cheema, *Acta Biomater*, 2013, **9**, 7917-7926.

17. R. A. Brown, M. Wiseman, C. B. Chuo, U. Cheema and S. N. Nazhat, *Adv Funct Mat*, 2005, **15**, 986-992.

18. U. Cheema and R. A. Brown, *Adv Wound Care*, 2013, **2**, 176-184.

19. M. Bitar, V. Salih, R. A. Brown and S. N. Nazhat, *J Mater Sci Mater Med*, 2007, **18**, 237-244.

20. J. L. Bailey, P. J. Critser, C. Whittington, J. L. Kuske, M. C. Yoder and S. L. Voytik-Harbin, *Biopolymers*, 2011, **95**, 77-93.

21. M. Marotta and G. Martino, *Anal Biochem*, 1985, **150**, 86-90.

22. ASTM Standard F3089-14, "Standard Guide for Characterization and Standardization of Polymerizable Collagen-Based Products and Associated Collagen-Cell Interactions," ASTM International, West Conshohocken, PA, 2014.

23. S. L. Voytik-Harbin, B. Rajwa and J. P. Robinson, *Methods Cell Biol*, 2001, **63**, 583-597.

24. A. O. Brightman, S. L. Voytik-Harbin, B.Z. Waisner, J.P. Robinson, C.H. Lamar, *Tissue Eng*, 1998, **4**, 157-174.

25. J. M. Wallace, Q. Chen, M. Fang, B. Erickson, B. G. Orr and M. M. Banaszak Holl, *Langmuir*, 2010, **26**, 7349-7354.

26. C. P. Neu, K. Komvopoulos and A. H. Reddi, *Tissue Eng Part B Rev*, 2008, **14**, 235-247.

27. I. V. Yannas, J. F. Burke, C. Huang and P. L. Gordon, *J Biomed Mater Res*, 1975, **9**, 623-628.

28. Y. S. Pek, M. Spector, I. V. Yannas and L. J. Gibson, *Biomaterials*, 2004, **25**, 473–482.

29. L. Besseau, B. Coulomb, C. Lebreton-Decoster and M. M. Giraud-Guille, *Biomaterials*, 2002, **23**, 27-36.

30. S. L. Voytik-Harbin and B. Han, in *CRC Handbook of Imaging in Biological Mechanics*, eds. C. P. Neu and G. M. Genin, CRC Press, Boca Raton, Florida, 2014, ch. 20, pp. 261-273.

31. D. T. Woodley, M. Yamauchi, K. C. Wynn, G. Mechanic and R. A. Briggaman, *J Invest Dermatol*, 1991, **97**, 580-585.

32. N. Kuznetsova and S. Leikin, *J Biol Chem*, 1999, 36083-36088.

33. K. E. Kadler, D. F. Holmes, J. A. Trotter and J. A. Chapman, *Biochem J*, 1996, **316**, 1-11.

34. A. Diaz-Gonzalez, M. A. Gallant, D. B. Burr and J. M. Wallace, *J Biomech*, 2014, **47**, 681-686.

35. M. A. Hammond, M. A. Gallant, D. B. Burr and J. M. Wallace, *Bone*, 2014, **60**, 26-32.

36. J. Wallace, *Connect Tissue Res*, 2015, **56**, 68-75.

37. M. A. Hammond and J. M. Wallace, *BoneKEy Rep*, 2015, **4**, 1-5.

38. T. Novak, B. Seelbinder, C. M. Twitchell, C. C. van Donkelaar, S. L. Voytik-Harbin and C. P. Neu, *Adv Funct Mat*, 2016 (in press).

39. E. A. Abou Neel, L. Bozec, J. C. Knowles, O. Syed, V. Mudera, R. Day and J. K. Hyun, *Adv Drug Deliv Rev*, 2013, **65**, 429-456.

40. E. Bell, B. Ivarsson and C. Merrill, *Proc Natl Acad Sci U S A*, 1979, **76**, 1274-1278.

41. W. Friess, *Eur J Pharm Biopharm*, 1998, **45**, 113-136.

42. D. P. Speer, M. Chvapil, C. D. Eskelson and J. Ulreich, *J Biomed Mat Res*, 2015, **14**, 753-764.

43. N. Anandagoda, D. G. Ezra, U. Cheema, M. Bailly and R. A. Brown, *J R Soc, Interface*, 2012, **9**, 2680-2687.

44. C. T. McKee, J. A. Last, P. Russell and C. J. Murphy, *Tissue Eng, Part B*, 2011, **17**, 155-164.

45. F. H. Silver, G. P. Seehra, J. W. Freeman and D. DeVore, *J Appl Polym Sci*, 2002, **86**, 1978-1985.

46. P. Angele, J. Abke, R. Kujat, H. Faltermeier, D. Schumann, M. Nerlich, B. Kinner, C. Englert, Z. Ruszczak, R. Mehrl and R. Mueller, *Biomaterials*, 2004, **25**, 2831–2841.

47. C. E. Ghezzi, N. Muja, B. Marelli and S. N. Nazhat, *Biomaterials*, 2011, **32**, 4761-4772.

48. F. Guilak, K. E. Lott, H. A. Awad, Q. Cao, K. C. Hicok, B. Fermor and J. M. Gimble, *J Cell Physiol*, 2015, **206**, 229-237.

49. J. M. Gimble and F. Guilak, *Cytotherapy* 2009, **5**, 362-369.

50. P. Carinci, M. Bodo, R. Evangelisti and E. Becchetti, *Ital J Anat Embryol*, 1995, **100 Suppl 1**, 65-74.

51. S. Rhee and F. Grinnell, *Adv Drug Deliv Rev*, 2007, **59**, 1299-1305.

52. A. M. Pizzo, K. Kokini, L. C. Vaughn, B. Z. Waisner and S. L. Voytik-Harbin, *J Appl Physiol*, 2005, **98**, 1909-1921.

53. T. Elsdale and J. Bard, *J Cell Biol*, 1972, **54**, 626-637.

54. G. Mosser, A. Anglo, C. Helary, Y. Bouligand and M. M. Giraud-Guille, *Matrix Bio*, 2006, **25**, 3–13.

55. L. Besseau and M. M. Giraud-Guille, *J Mol Bio*, 1995, **251**, 197–202.

56. N. Saeidi, K. P. Karmelek, J. A. Paten, R. Zareian, E. DiMasi and J. W. Ruberti, *Biomaterials*, 2012, **33**, 7366–7374.

57. D. P. Knight, L. Nash, X. W. Hu, J. Haffegee and M. W. Ho, *J Biomed Mater Res*, 1998, **41**, 185-191.

58. E. A. Abou-Neel, U. Cheema, J. C. Knowles, R. A. Brown and S. N. Nazhat, *Soft Mat*, 2006, **2**, 986-992.

59. B. Marelli, C. E. Ghezzi, M. James-Bhasin and S. N. Nazhat, *Biomaterials*, 2015, **37**, 183–193.

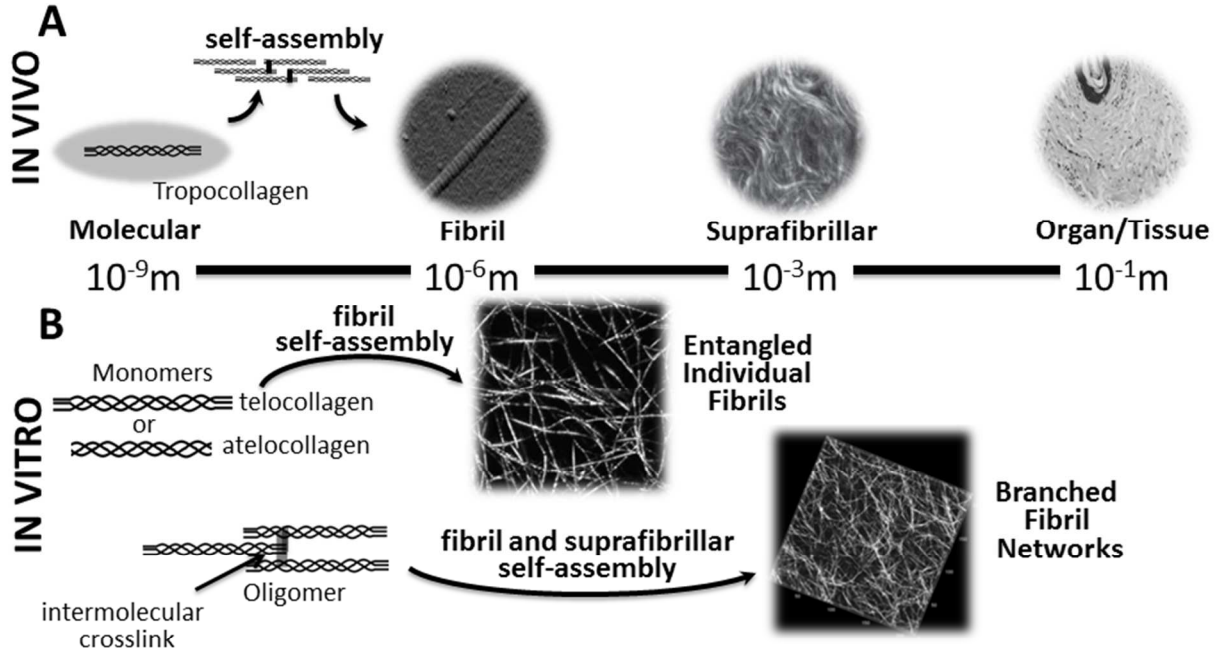

Figure 1. Hierarchical, multi-scale organization of type I collagen as occurs (A) *in vivo* and (B) *in vitro* with polymerizable monomer (atelocollagen and telocollagen) and oligomer formulations.

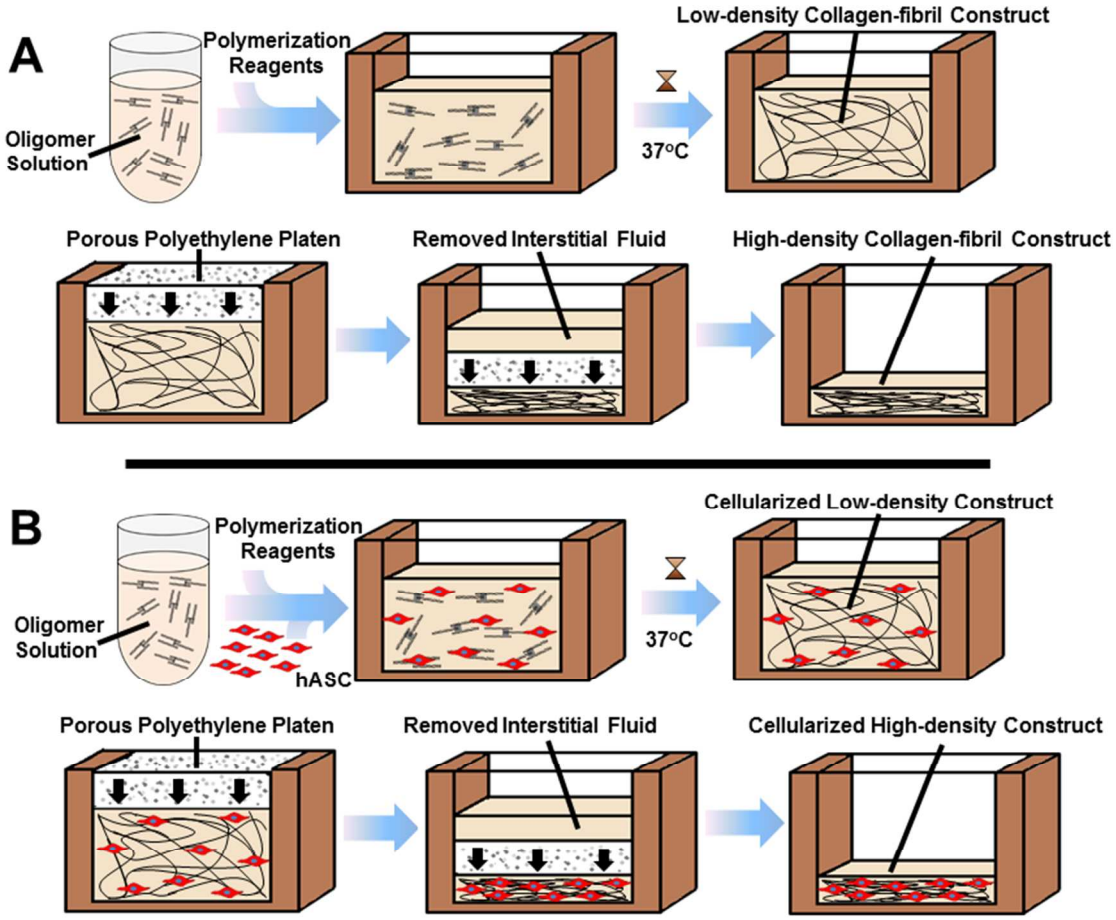

Figure 2. Process diagrams for preparation of (A) high-density collagen-fibril constructs and (B) cellularized high-density tissue constructs.

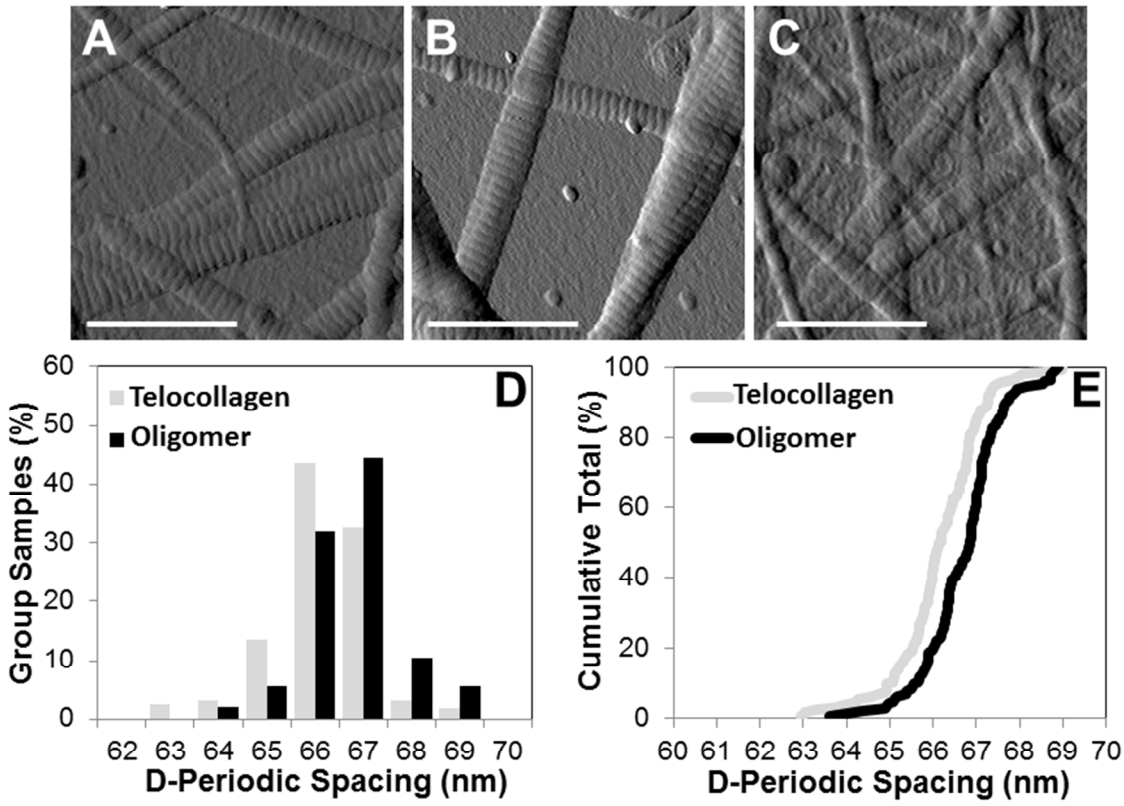

Figure 3. High resolution AFM images confirm that low-density oligomer matrices represent highly interconnected fibril networks with D-periodic spacing resembling those found *in vivo*. Representative AFM error images show prominent D-periodic spacing patterns for (A) oligomer and (B) telocollagen but not (C) atelocollagen, all polymerized at 0.5 mg/mL. (D) Histogram plot and (E) cumulative density function show statistically significant increase in D-periodic spacing distribution for oligomer versus telocollagen as determined by the Kolmogorov-Smirnov test ($p<0.05$). Scale bar = 1μm

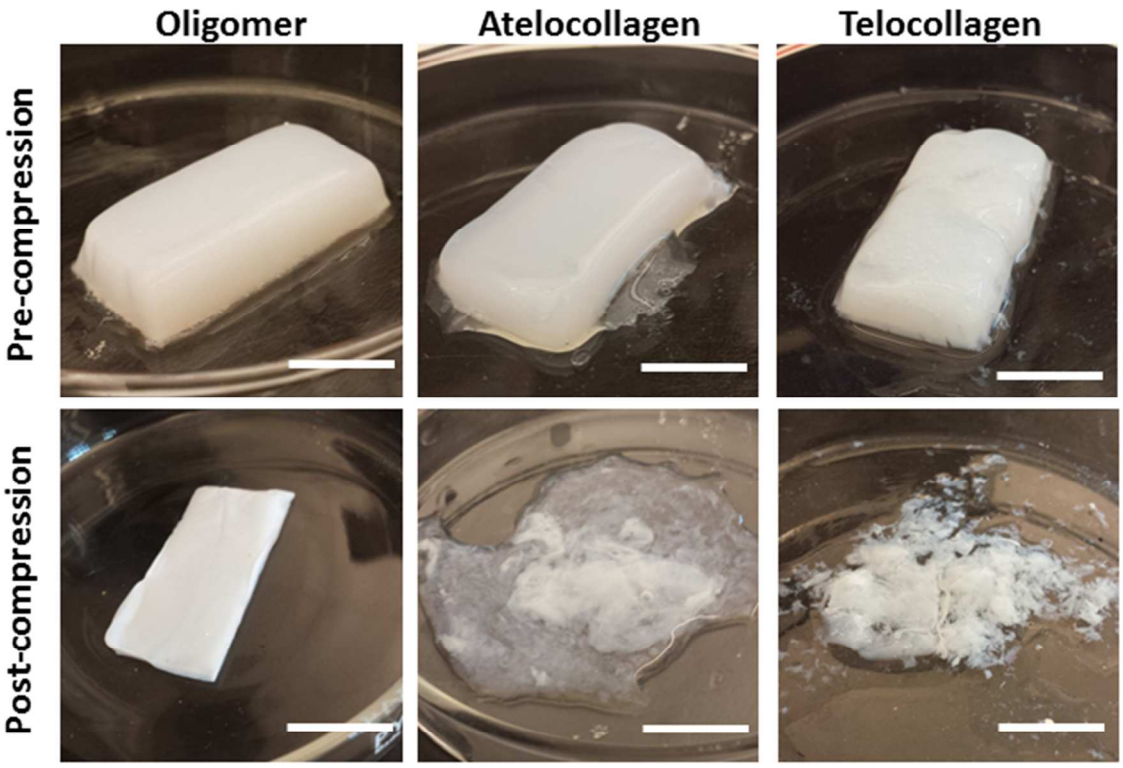

Figure 4. Representative images of oligomer, atelocollagen, and telocollagen constructs before (3.5 mg/mL) and after (24.5 mg/mL) confined compression (86% strain or 7X). Scale bars = 2 mm

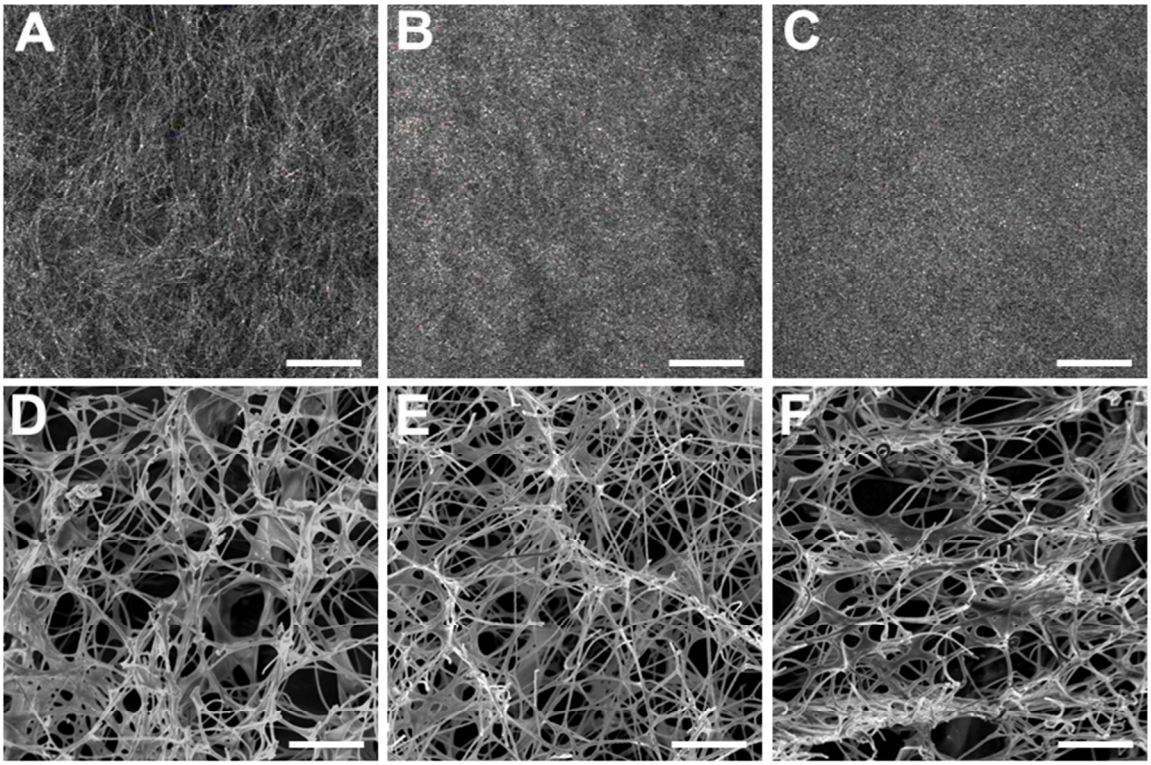

Figure 5. Fibril microstructure and ultrastructure of collagen-fibril constructs prepared at final oligomer concentrations of 3.5 mg/mL (A,D), 12.25 mg/mL (B,E), and 24.5 mg/mL (C,F) as visualized using confocal reflection microscopy (A-C) and cryo-SEM (D-F). Scale bars for A-C and D-F represent 20 μm and 4 μm, respectively.

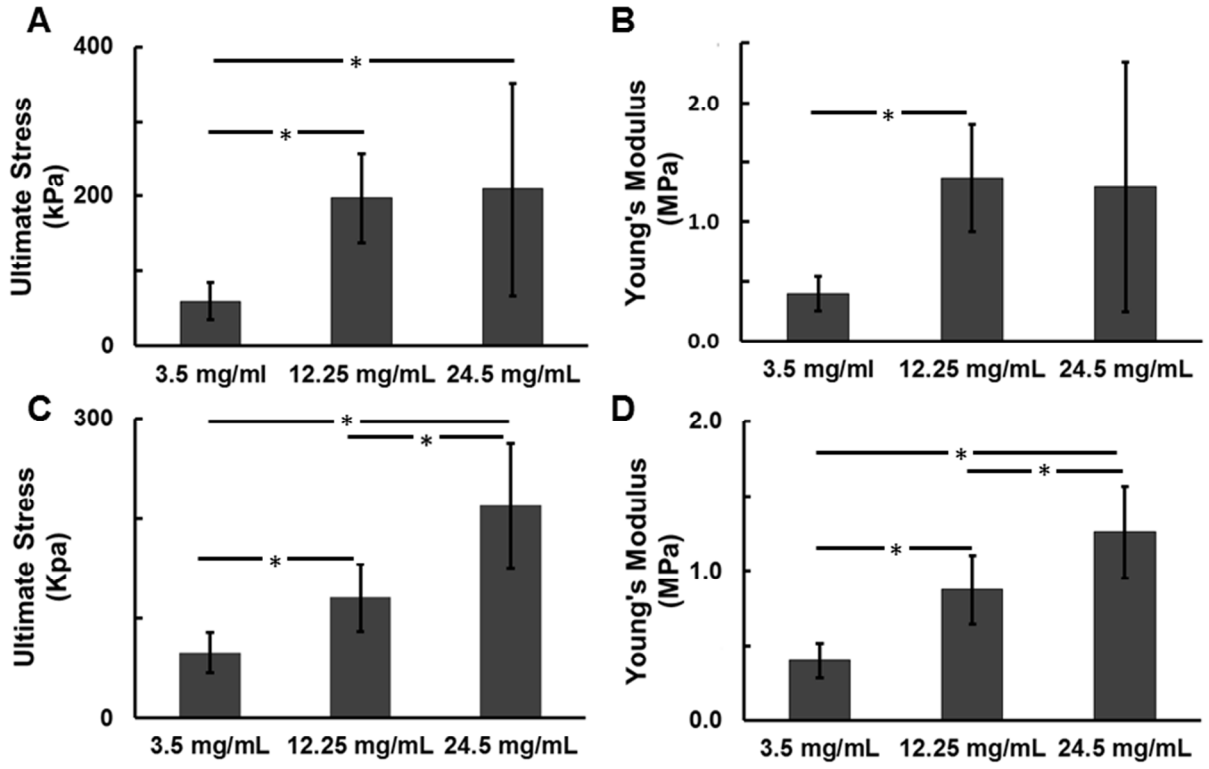

Figure 6. Engineering tensile properties of 3.5 mg/mL, 12.25 mg/mL, and 24.5 mg/mL oligomer constructs following 1 hour (A,B) or 18 hour (C,D) polymerization. Dog-bone shaped samples with gauge length, width, and thickness of 10 mm, 4 mm, and 2 mm, respectively, were subjected to uniaxial tensile loading and ultimate stress (A,C), Young's modulus (B,D), and failure strain (not shown) measured (data represents mean±SD; $n=7$). * denotes statistically significant difference ($p<0.05$). Table 2 provides summary of measured values for 18-hr constructs.

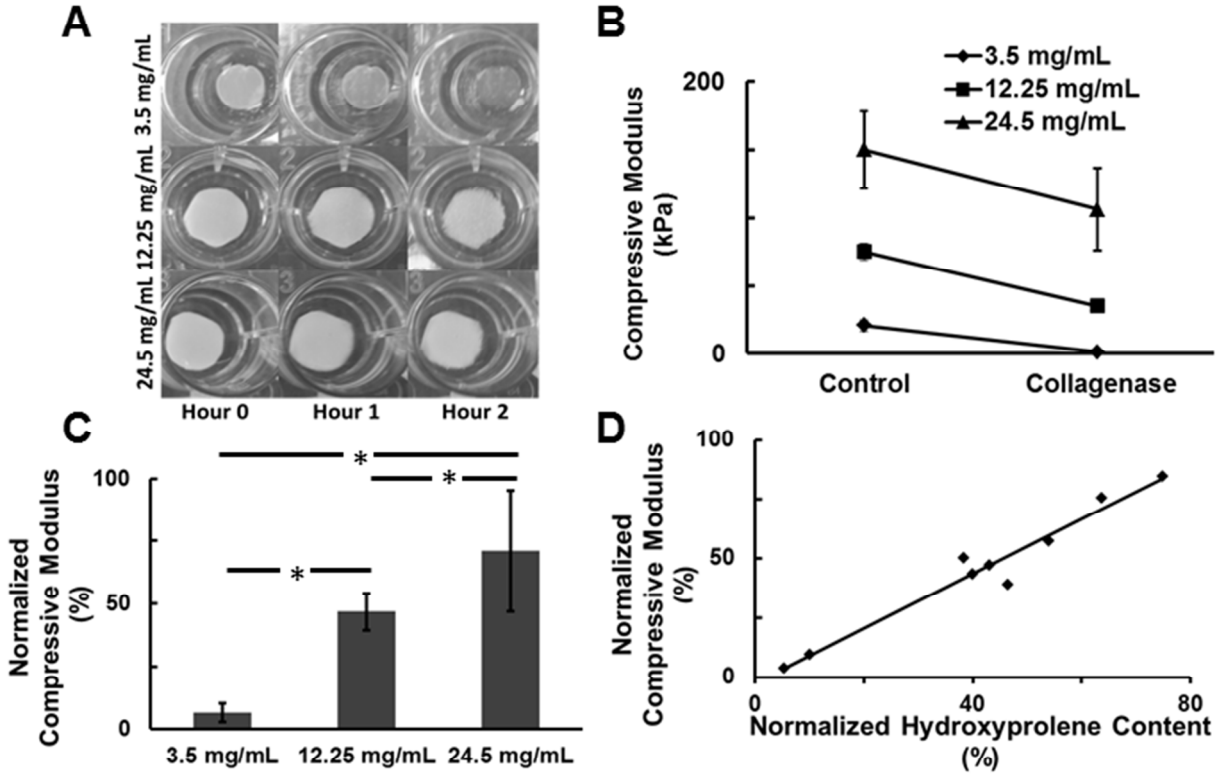

Figure 7. Density-dependent collagenase degradability of oligomer constructs. (A) Temporal changes in oligomer constructs prepared at 3.5 mg/mL, 12.25 mg/mL, and 24.5 mg/mL following collagenase (31.2 U/mL) treatment. Scale bar = 1 cm. (B) Compressive modulus of untreated (control) and collagenase-treated (2 hr) constructs (data represents mean±SD; $n=7$). (C) Compressive modulus of collagenase-treated constructs normalized to control construct values (data represent mean±SD; $n=7$). * denotes statistically significant difference ($p<0.05$). (D) Relationship between compressive modulus and hydroxyproline content values for collagenase-treated constructs. Values are normalized to control construct values.

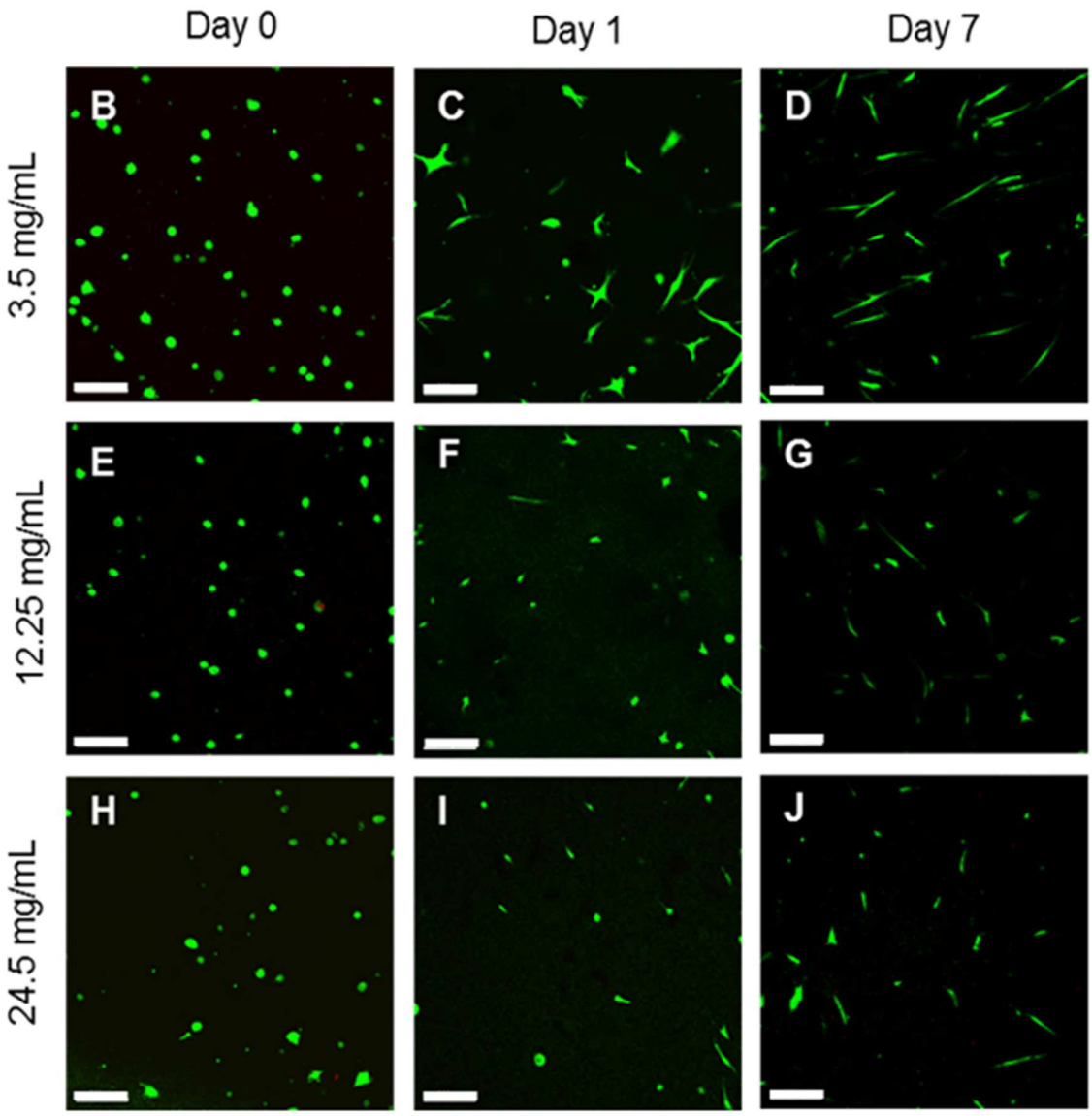

Figure 8. Human ASC maintain high cell viability over time within high-density collagen-fibril constructs. Human ASC were seeded in oligomer matrices (3.5 mg/mL) at $5x10^5$ cells/mL and then densified to 3.5 mg/mL, 12.25 mg/mL, and 24.5 mg/mL. Constructs were stained with Calcein-AM (green) and PI (red) to assess cell viability and visualized using confocal microscopy. Images represent 2D projection of image stacks (50 μm). Scale bars = 200 μm

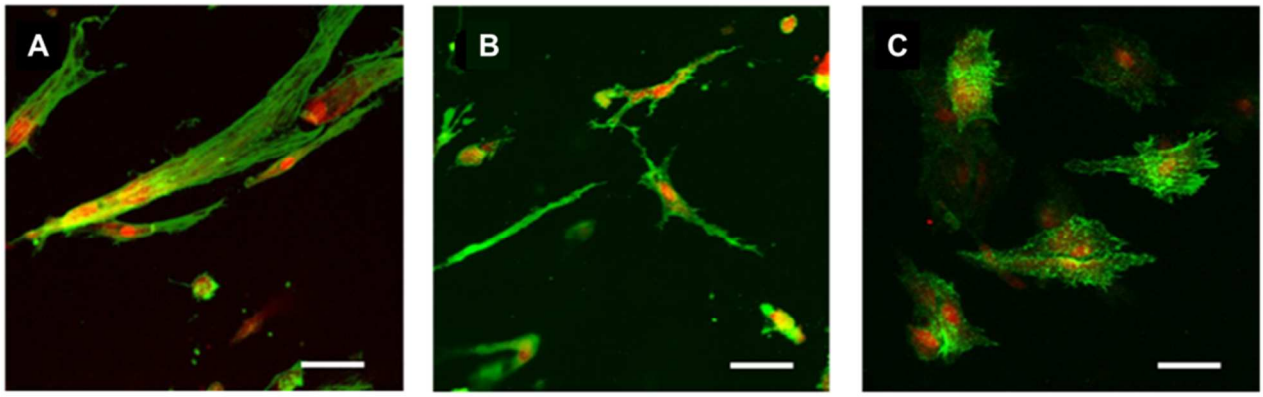

Figure 9. Human ASC morphology and cytomechanics varies with oligomer construct density. Representative images of hASC within 3.5 mg/mL (C), 12.25 mg/mL (D), and 24.5 mg/mL (E) constructs stained with phalloidin (green) and DRAQ5 (red), and visualized using confocal microscopy. Images represent 2D projections of image stacks (50 μm). Scale bars = 50 μm

Table 1. Summary of methods for creating high-density collagen constructs in the presence and absence of cells.

Process	Neutralization	Final Formulation	Mechanical Properties	Cell Encapsulation	Ref
concentration of soluble collagen by centrifugation followed by polymerization; 90 min	PBS	10-20 mg/mL constructs	up to 70 kPa Young's modulus	yes	13, 53
continuous injection/ evaporation; weeks to months	ammonia vapor	thin matrices up to 1000 mg/mL	not shown	no	54, 55
reverse dialysis with PEG prior to polymerization; 24 hours	Titration of PEG	375 mg/mL	not shown	no	56, 57
polymerization of low-concentration telocollagen followed by unconfined compression/absorption; 5 min	DMEM and NaOH	dense thin sheets (~98% weight loss)	up to 4 MPa Young'smodulus	yes, cell death with high strain compression	17, 19, 58
polymerization of low-concentration telocollagen followed by aspiration and ejection; 15 min	DMEM and NaOH	anisotropic collagen rods of 45.5 mg/mL	not shown	yes	59

Table 2. Summary of engineering tensile properties for oligomer constructs

Oligomer Concentration (mg/mL)	Engineering Ultimate Stress (kPa)	Failure Strain (%)	Engineering Young's Modulus (MPa)
3.5	65.7±20.4	27.1±2.6	0.40±0.12
12.25	120.8±33.7	26.1±4.2	0.88±0.23
24.5	212.9±62.2	30.4±4.1	1.26±0.31

TABLE OF CONTENTS ENTRY

Integrated use of collagen oligomers and confined compression for design of acellular and cellular high-density, collagen-fibril constructs with suprafibrillar organization